

Inertial Sensor-Based State Estimation of Flexible Links Subject to Bending and Torsion

Petri Mäkinen, Teemu Mononen and Jouni Mattila

Laboratory of Automation and Hydraulic Engineering

Tampere University of Technology

Tampere, Finland

Emails: petri.makinen@tut.fi, teemu.mononen@tut.fi, jouni.mattila@tut.fi

Abstract—In this study, we propose an observer design based on inertial sensors and the finite element (FE) method to estimate the flexural states of a long-reach and highly flexible manipulator in a 3D plane of motion. Vertical and lateral dynamic bendings are considered, along with deformation due to torsion. The aim is to achieve accurate end-point positioning by using the estimated flexural degrees-of-freedom, which are formulated using an FE model. The states are reconstructed based on angular velocity measurements, which are obtained from strap-on inertial sensors placed along the flexible link. For validation, a motion-capture setup consisting of three OptiTrack cameras is used. The experiments are conducted on a hydraulic manipulator that has a single 4.5-m long flexible link with a tip mass. The validation is carried out by comparing the estimates to the OptiTrack reference measurements. The results demonstrate that this method provides satisfactory end-point positioning, while also being convenient for use in heavy-duty mobile manipulators.

Index Terms—inertial sensors, state estimation, finite element method

I. INTRODUCTION

Robotic systems are widely expected to dominate in the near future with increasingly autonomous functions. For example, significant efforts have been and are being made in the mass consumer sector to establish self-driving cars. In this robotic revolution, this self-maneuverability is expected to shift to smaller industrial sectors involving heavy-duty working machines, such as excavators and forestry machines, which are equipped with robotic manipulators. In mobile (off-highway) machines, weight has a significant effect on fuel consumption and productivity. Therefore, it is also expected that materials such as high-strength steel alloys will become more common as construction materials in mobile manipulators, because lighter structures can be manufactured from these materials. Although the strength of the material is augmented, its elastic modulus does not typically change. This means that the material can withstand higher loads with less weight, but the elastic deformations caused by the higher loads are also greater. Thus, to fully utilize these materials, it is necessary to address the flexibility in the control design.

With rigid manipulators (e.g., industrial robots), which are purposely constructed to be as stiff as possible, the end-point position can be formulated utilizing joint angle measurements, resulting in an accurate end-point position. With flexible manipulators, however, the dynamic end-point formulation

becomes much more challenging due to the structural deformations, such as bending and torsion. A measurement or an estimate of the end-point position is required for successful control implementations. Many state-of-the-art model-based control methods (backstepping, virtual decomposition control, and integral resonant control) developed for flexible-link robotics assume that the end-point position can be measured or estimated to enable control feedback [1]–[5]. Moreover, many of these studies present only simulation results, where the lack of an accurate end-point position measurement is not a real issue.

A wide variety of sensors have been employed in the task of measuring the end-point position of a flexible link, as [6] and a survey paper on the control and sensor systems of flexible manipulators [7] presented. Some of the most studied methods are vision- and strain-gauge-based systems. The most common method of deformation sensing is a strain gauge. However, it can measure only local deformations and is susceptible to disturbances and biases from temperature variations and electromagnetic interferences. Due to these practical difficulties, strain gauges are mostly employed for vibration damping (see, for example, [8], [9]) instead of deformation sensing.

As a result of the increase in raw computing power, in the last few decades many research groups have focused on vision-based estimation systems. Vision sensor data was used to estimate the state variables of a flexible link robot in [10]. Two separate observers were used: one for fast dynamics using strain gauges and another for slow dynamics using a camera. In [11], a two-time scale controller was proposed for the end-point control of a flexible beam. The tip position was obtained directly from vision data, while the vision signal, subject to delays, was compensated by a state estimator and a predictor. The main drawback with visual sensing is the time delay between capturing an image and processing it [7]. Visual measuring devices are also vulnerable to disruptions, particularly outdoors. Furthermore, only a few studies, such as [12] and [13], focused on long-reach flexible manipulators. Typical robotic manipulators used in mobile machines are large-scale and long reaching. It is also clear that there is a lack of practical studies considering a 3D plane of motion.

More recently, inertial sensing schemes have generated a considerable amount of interest in rigid body robotics. For example, inertial sensors were used for estimating the joint

states of humanoid robots in [14] and [15]. In [16], inertial sensors were used in a heavy-duty hydraulic manipulator for motion feedback estimation. In [17], an inertial sensor-based scheme was proposed for rotary joint angle estimation of rigid body mobile manipulators. A gravity-referenced joint angle estimation method for heavy-duty manipulators using three-axis accelerometers and three-axis rate gyros was proposed in [18].

In this paper, a state observer based on inertial sensor measurements and the finite element (FE) method is proposed to estimate the flexural degrees-of-freedom (DOF) of a flexible link in a 3D plane of motion. It is shown that the system is fully observable. The rigorous stiffness and inertia relations of the FE method enable the estimation of deflections from velocity measurements, obtained from microelectromechanical system (MEMS) inertial measuring units (IMUs). Reconstructing the flexural states is based on the angular velocities measured using triaxial IMUs placed along the flexible link. The IMU type used is by Analog Devices and it includes a hermetic seal with factory-calibrated characteristics for each sensor, including sensitivity, bias, and alignment. The IMUs have a 6°/hr in-run bias stability and an operational temperature range of -40° to +105° Celsius. The sensors themselves are also enclosed in IP67 protected cases, which can easily be retrofitted in mobile manipulators.

This work is an extension of our previous study [19], in which we considered the inertial sensor-based FE state estimation scheme for a simple case of a 1-DOF long-reach flexible manipulator in a 2D plane of motion. In the present work, we extend and experimentally verify the estimation scheme for flexible links subject to bending and torsion in a 3D plane of motion.

This paper is outlined as follows: The beam model is presented in Section II, the observer design is described in Section III, the end-point position is formulated in Section IV, the experimental setup is presented in Section V, the results are given in Section VI, and the conclusion is presented in Section VII.

II. BEAM MODEL

A. Bending Deformation

The flexible link is modeled using the well-known Euler-Bernoulli beam theory, which incorporates a number of assumptions [20]: i) The cross-section of the beam is presumed infinitely rigid in its local plane. ii) After deformation, the cross-section remains plane. iii) After deformation, the cross-section also remains normal to the deformed axis of the beam. Due to the assumptions, the Euler-Bernoulli beam equation holds in the case of small deformations. The gravitational forces due to the beam's own mass are also excluded. In this study, vertical and lateral bendings of the beam are considered. The infinite-dimensional flexible beam is then

truncated into finite dimensions using the FE method. First, six shape functions are defined [21] for spatial interpolation:

$$N_1(x) = \frac{l-x}{l}, \quad N_2(x) = \frac{x}{l} \quad (1)$$

$$N_3(x) = 1 - \frac{3x^2}{l^2} + \frac{2x^3}{l^3}, \quad N_4(x) = x - \frac{2x^2}{l} + \frac{x^3}{l^2} \quad (2)$$

$$N_5(x) = \frac{3x^2}{l^2} - \frac{2x^3}{l^3}, \quad N_6(x) = -\frac{x^2}{l} + \frac{x^3}{l^2} \quad (3)$$

where l denotes the length of an element. The vertical and lateral stiffness matrix components for an element are defined as follows:

$$\mathbf{K}_e^y = \int_0^l H_y^T E I_z H_y dx \quad (4)$$

$$\mathbf{K}_e^z = \int_0^l H_z^T E I_y H_z dx \quad (5)$$

where I_z and I_y denote the moments of inertia, and E denotes the elastic modulus. The shape function vectors H_y and H_z are given as:

$$H_y = [N_3''(x), N_4''(x), N_5''(x), N_6''(x)] \quad (6)$$

$$H_z = [N_3''(x), -N_4''(x), N_5''(x), -N_6''(x)] \quad (7)$$

where an apostrophe denotes differentiation with respect to the spatial variable x . The element inertia matrices are defined as follows:

$$\mathbf{M}_e^y = \rho A \int_0^l N_y^T N_y dx \quad (8)$$

$$\mathbf{M}_e^z = \rho A \int_0^l N_z^T N_z dx \quad (9)$$

where ρ denotes the mass per unit length, A denotes the cross-sectional area, and N_y and N_z are vectors containing the shape functions:

$$N_y = [N_3(x), N_4(x), N_5(x), N_6(x)] \quad (10)$$

$$N_z = [N_3(x), -N_4(x), N_5(x), -N_6(x)]. \quad (11)$$

B. Torsional Deformation

The element stiffness and inertia matrices due to torsion can be written as follows [21]:

$$\mathbf{K}_e^{\theta_x} = \int_0^l B^T G I_x B dx, \quad \mathbf{M}_e^{\theta_x} = I_t \int_0^l N_x^T N_x dx \quad (12)$$

where G denotes the shear modulus, I_x denotes the torsional moment of inertia, and I_t denotes the mass moment of inertia per unit length. The shape function vectors are formulated as follows:

$$B = [N_1'(x), N_2'(x)], \quad N_x = [N_1(x) \ N_2(x)]. \quad (13)$$

C. Tip Mass

The kinetic energy for the tip mass can be expressed as follows:

$$E_k = \frac{1}{2}mv_c^2 + \frac{1}{2}\omega^T \mathbf{J}_c \omega \quad (14)$$

where m denotes the tip mass, v_c denotes the velocity vector with respect to the center of mass of the tip mass, ω denotes the vector of angular velocities at the tip, and \mathbf{J}_c denotes an inertia matrix, formulated as follows:

$$\mathbf{J}_c = \begin{bmatrix} \frac{mr^2}{4} + \frac{mh^2}{12} & 0 & 0 \\ 0 & \frac{mr^2}{4} + \frac{mh^2}{12} & 0 \\ 0 & 0 & \frac{mr^2}{2} \end{bmatrix}. \quad (15)$$

Here, the tip mass is assumed to be cylindrical, with r denoting the radius and h denoting the thickness. The velocity vector of the center of mass of the tip mass is given as follows:

$$v_c = [v_x \ v_y \ v_z] + [\omega_x \ \omega_y \ \omega_z] \times [s_x \ s_y \ s_z] \quad (16)$$

where s_x , s_y , and s_z denote shifts from the center axis of the beam, allowing an asymmetric tip mass with respect to the beam's symmetry axis. The linear and angular velocities (v_x , v_y , v_z , ω_x , ω_y , ω_z) are measured from the neutral axis of the link and at the tip. The full 6×6 tip mass matrix can then be written as follows:

$$\mathbf{M}_{point} = \frac{\partial^2 E_k}{\partial \dot{q}_i \partial \dot{q}_i^T} \quad (17)$$

where

$$\dot{q}_t = [v_x \ v_y \ v_z \ \omega_x \ \omega_y \ \omega_z]^T. \quad (18)$$

As axial compressibility is not considered in this work, the matrix is reduced to 5×5 by removing the first row and column, and then summed to the inertia matrix of the last finite element's second node (located at the tip of the beam).

D. System Equation

Combining the bending and torsional deformations by using standard FE method procedures, the dynamic equation for an element can be written as follows:

$$\mathbf{M}_e \ddot{q}_e + \mathbf{K}_e q_e = F_e(t) \quad (19)$$

$$q_e = [v_{e1} \ w_{e1} \ \theta_{ex1} \ \theta_{ey1} \ \theta_{ez1} \ v_{e2} \ w_{e2} \ \theta_{ex2} \ \theta_{ey2} \ \theta_{ez2}]^T \quad (20)$$

where the element inertia matrix is denoted by \mathbf{M}_e , the element stiffness matrix is denoted by \mathbf{K}_e , and $F_e(t)$ denotes dynamic forces affecting a given element. The vector of the nodal coordinates contains five DOF for the left-hand node of an element and another five for the right-hand node, respectively. Vertical deflection is denoted by v_e , lateral deflection is denoted by w_e , rotation about the X-axis of the beam is denoted by θ_{ex} , rotation about the Y-axis of the beam is denoted by θ_{ey} , and rotation about the Z-axis of the beam is denoted by θ_{ez} . Using typical FE analysis procedures, the global matrices for the beam are built by combining the

element matrices. The global dynamic equation is expressed as follows:

$$\mathbf{M} \ddot{q} + \mathbf{K} q = F \bar{u}(t) \quad (21)$$

where the global inertia matrix is denoted by \mathbf{M} , and the global stiffness matrix is denoted by \mathbf{K} . The external force vector is denoted by F and the input defining vector by $\bar{u}(t)$. The global nodal coordinate vector q is defined by (22). The vertical force and the torsional moment are induced to the last node by the tip mass, which is defined in (23). The bulk of the force and the moment are placed in the input vector $\bar{u}(t)$.

$$q = [v_1 \ w_1 \ \theta_{x1} \ \theta_{y1} \ \theta_{z1} \ \dots \ v_i \ w_i \ \theta_{xi} \ \theta_{yi} \ \theta_{zi}]^T \quad (22)$$

$$F = \begin{bmatrix} 0 & 0 & 0 & 0 & \dots & 1 & 0 & 0 & 0 & 0 \\ 0 & 0 & 0 & 0 & \dots & 0 & 0 & 1 & 0 & 0 \end{bmatrix}^T \quad (23)$$

Here $1, \dots, i$ denotes the node index. In order to realize the mechanical boundary constraints of the system, the translational and torsional DOF of nodes 1 (the rotary joint axis) and 2 (the cylinder attachment point) are constrained to zero. For computational efficiency, the second-order dynamic equation (21) is reduced into a first-order form using a state-space representation. For this purpose, the constrained nodes are removed completely from the model. The first-order form is formulated as follows:

$$\dot{x} = \frac{d}{dt} \begin{bmatrix} q_r \\ \dot{q}_r \end{bmatrix} = \begin{bmatrix} \mathbf{0} & \mathbf{I} \\ -\mathbf{M}_r^{-1} \mathbf{K}_r & \mathbf{0} \end{bmatrix} \begin{bmatrix} q_r \\ \dot{q}_r \end{bmatrix} + \begin{bmatrix} \mathbf{0} \\ \mathbf{M}_r^{-1} F_r \end{bmatrix} u \quad (24)$$

where subscript r denotes a reduced matrix or vector, in which the degrees of freedom of the two constrained nodes are removed. The identity matrix is denoted by \mathbf{I} . The expression (24) is equivalent to the generic state-space representation:

$$\begin{cases} \dot{x} = \mathbf{A}x + \mathbf{B}u \\ y = \mathbf{C}x + \mathbf{D}u \end{cases} \quad (25)$$

where x contains the system states, and u contains the system inputs. Let n indicate the number of finite elements. The dimensions of the matrices are: \mathbf{A} is $10n \times 10n$, \mathbf{B} is $10n \times inputs$, \mathbf{C} is $outputs \times 10n$, and \mathbf{D} is $outputs \times inputs$.

III. OBSERVER DESIGN

The observability of the system states was first confirmed by using the Popov-Belevitch-Hautus test for observability [22]:

$$\text{rank} \begin{bmatrix} \mathbf{C} \\ \lambda \mathbf{I} - \mathbf{A} \end{bmatrix} = 10n \quad (26)$$

where $\lambda \in \mathbb{C}$ is a vector consisting of the eigenvalues of the system. Clearly, the rank is full, meaning all the system states can be reconstructed using a state observer. The observer design is formulated as follows:

$$\begin{cases} \dot{\hat{x}} = \mathbf{A}_{obs} \hat{x} + \mathbf{B}_{obs} u^* \\ \hat{y} = \mathbf{C}_{obs} \hat{x} + \mathbf{D}_{obs} u^* \end{cases} \quad (27)$$

with $u^* = [y^T \ | \ u^T]^T$. Here, $\hat{(\cdot)}$ denotes a vector of estimated variables. The matrices are defined as follows:

$$\mathbf{A}_{obs} = \mathbf{A} - (\mathbf{G}^T \mathbf{C}), \quad \mathbf{B}_{obs} = [\mathbf{G}^T \ | \ \mathbf{B}] \quad (28)$$

$$\mathbf{C}_{obs} = \mathbf{I}, \quad \mathbf{D}_{obs} = \mathbf{0} \quad (29)$$

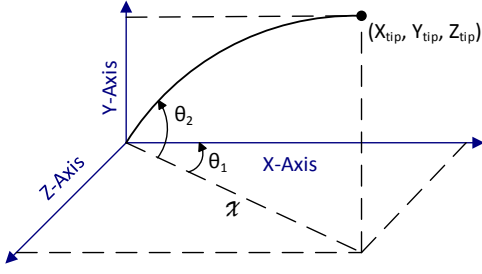


Fig. 1. The end-point position of the flexible link. Vertical and horizontal bendings are accounted for.

where \mathbf{G} is the observer gain matrix. The dimensions of the observer matrices are: \mathbf{A}_{obs} is $10n \times 10n$, \mathbf{B}_{obs} is $10n \times inputs$, \mathbf{C}_{obs} is $outputs \times 10n$, and \mathbf{D}_{obs} is $outputs \times inputs$. Compared to (24), the amounts of the inputs and outputs change.

The observer gain matrix \mathbf{G} is obtained based on the dualistic property [21] between a state observer and state feedback. An algebraic Riccati equation (ARE) is solved using the linear quadratic regulator algorithm, while considering the dualism by replacing \mathbf{A} with \mathbf{A}^T and \mathbf{B} with \mathbf{C}^T . The Riccati matrix \mathbf{S} is solved from the following ARE:

$$\mathbf{S}\mathbf{A}^T + \mathbf{A}\mathbf{S} - \mathbf{S}\mathbf{C}^T\mathbf{R}^{-1}\mathbf{C}\mathbf{S} + \mathbf{Q} = 0. \quad (30)$$

The observer gain matrix \mathbf{G} is finally obtained as follows:

$$\mathbf{G} = \mathbf{R}^{-1}\mathbf{C}\mathbf{S} \quad (31)$$

where two weighting factors are denoted by \mathbf{Q} and \mathbf{R} .

IV. CARTESIAN POSITION FORMULATION

The Cartesian coordinates of the flexible link are illustrated in Fig. 1. First, the length of the flexible link in the XZ-plane, denoted by \mathcal{X} , is formulated as follows:

$$\mathcal{X} = L_i \cos(\theta_2) - v_i \sin(\theta_2) \quad (32)$$

where L_i denotes the length of an undeformed link, v_i denotes the estimated vertical deflection at a given point along the link, and θ_2 denotes the lift angle. Based on trigonometry, a Cartesian position along the flexible link can then be derived as follows:

$$X_c = \mathcal{X} \cos(\theta_1) + w_i \sin(\theta_1) \quad (33)$$

$$Y_c = L \sin(\theta_2) + v_i \cos(\theta_2) + h_0 \quad (34)$$

$$Z_c = \mathcal{X} \cos(\pi/2 - \theta_1) - w_i \cos(\theta_1) \quad (35)$$

where θ_1 denotes the turn angle, w_i denotes the estimated lateral deflection at a given point along the link, and h_0 denotes the pillar height.

V. EXPERIMENTAL SETUP

Two experimental manipulators were used in the experiments. A 1-DOF manipulator is presented in Fig. 2, and a 2-DOF manipulator is presented in Fig. 3. Most of the experiments were conducted on the 1-DOF system due to it

having considerably less backlash in the lateral plane. The 2-DOF manipulator was used to test dynamic end-point tracking in Cartesian (X,Y,Z) space using the estimated deformations.

Both manipulators have identical 4.5-m long flexible links that are actuated by hydraulic cylinders. The material used in the links is a high-strength steel with a yield strength of 700 MPa and an ultimate strength of 750–950 MPa. Thus, the manipulators can withstand considerable elastic deformations without permanent structural changes. The angles of the revolute joints are measured using Heidenhain ROD 480 5000 27S12-03 incremental encoders. The pair of cylinders actuating the turn joint in the 2-DOF manipulator are sized $\varnothing 40/20-150$, whereas the lift cylinder is sized $\varnothing 40/20-200$. The lift cylinder of the 1-DOF manipulator is sized $\varnothing 35/25-300$. Three Bosch Rexroth 4WRPEH servo valves with nominal flows of 40 dm³/min are used, along with a supply pressure of 17 MPa. The inertial sensors were based on an ADIS16485 *iSensor*[®] chip, which measures angular velocities (range $\pm 450^\circ/\text{sec}$) and accelerations (range $\pm 5g$) with respect to three different axes. A dSPACE controller board with ControlDesk software was used for the real-time implementation.

The flexible link was divided into six finite elements so that the first node was located at the rotating joint axis and the second node was located at the cylinder attachment point (see Fig. 3). The remaining five nodes (3–7) were placed equally along the rest of the link, and each was assigned an IMU. Our previous study [19], which considered a planar flexible manipulator with vertical bending only, indicated that the location of the sensor, or the number of sensors, does not have a significant effect on the estimation accuracy. Thus, in this study we used a constant number of two IMUs, located at nodes 3 and 6, to provide inputs to the observer. The observer input vector u^* consisted of three angular velocities from each IMU, along with the force and moment induced by the tip mass. The alignment of the load force was formulated based on the measured lift angle and estimated rotation around the Z-axis at the tip of the flexible link.

To validate the estimation accuracy, a motion capture system was set up to record the bending profile of the flexible manipulator in Cartesian space. Three OptiTrack Prime 17W cameras were calibrated to capture reflective markers placed along the link. Specifically, markers were attached to nodes 3, 5, and 7. The cameras were placed in different positions and angles with respect to the manipulator in order to gain a more accurate capture result. For the camera setup, the world coordinate frame was set to be that of the manipulator (situated at the bottom of the pillar). The cameras sent data at 120 frames per second to a laptop running OptiTrack Motive and Matlab software. The data was preprocessed and then forwarded to a dSPACE controller board using UDP to record the end-point position in real-time.

For torsional measurements, a different setup was used: A marker was placed directly at the tip of the link (perpendicularly with respect to the link's symmetry axis), and the OptiTrack cameras were used to capture the rotation

angle of the tip due to torsion. First, a zero tip mass was used to calibrate the measured angle to zero, after which an asymmetric tip mass was added.

VI. RESULTS

In order to verify the observer's capability to estimate the flexural DOF along the link, a series of experiments was conducted by setting the flexible link of the 1-DOF manipulator to vibrate freely in different directions. The estimated deformations were compared to the OptiTrack reference measurements, whereas the estimated angular velocities were compared to the respective IMU measurements. Actual material parameters were used when formulating the observer equations.

Free vibration using a 20 kg tip mass was first experimented with. The results are illustrated in Fig. 4 and in Fig. 5. The left columns in the figures demonstrate vertical free vibration, whereas the right columns represent lateral free vibration. The black lines denote the OptiTrack reference measurements in Cartesian space, and the red lines denote the estimated Cartesian coordinates, formulated according to (34) and (35). The phases of the signals match perfectly, while the amplitudes are also closely matched. The increased difference in the amplitudes of the lateral vibration is mostly explained by the backlash in the experimental system in the lateral direction, meaning all the motion registered by the OptiTrack cameras is not due to elastic deformation of the link. The estimated and measured angular velocities also correspond to each other very well. Note that the estimated and measured angular velocities at nodes 3 and 6 (not illustrated) are identical because the velocities are used as input measurements to the observer.

Similar measurements were then conducted using a 40 kg tip mass, and the results are illustrated in Fig. 6 and in Fig. 7. The only parameter changed in the observer model was the tip mass, which was set to 40 kg instead of 20 kg. The results verify that the observer performs well using actual system parameters and with varying tip mass. The results also show that the amplitude of the vertical deflection at the tip is nearly 30 cm with a 40 kg tip mass.

An asymmetric tip mass was used to induce a torsional moment to the flexible link, after which the estimated and measured rotational angles due to torsion were compared. The results for 20 kg and 40 kg load masses are illustrated in Fig. 8. The results are in line with the previous bending estimation measurements: The phases match well, but the amplitudes of the estimates are decreased in comparison to the OptiTrack references. Note that the initial estimated (and measured) angle is nonzero due to the asymmetric tip mass. The OptiTrack reference measurement with a 40 kg tip mass also lost tracking of the marker at times. However, the wave form is still visible and clearly corresponds to the results using a 20 kg tip mass.

Finally, the 2-DOF manipulator was used for an end-point position tracking experiment to demonstrate that the estimated tip position, formulated using (33)-(35), matches the OptiTrack reference measurements in a 3D plane of motion. The results for three different tip masses are presented in Fig. 9, whereas

in Fig. 10 a sine reference is added. The figure shows the estimated Cartesian positions match well with their respective OptiTrack reference measurements. A simple proportional-integral (PI) controller and a slow reference trajectory were used in the implementation.

VII. CONCLUSION

In this study, an inertial sensor-based state estimation scheme using the FE method was proposed for estimating the flexural states of a long-reach flexible link in a 3D plane of motion. Vertical and lateral dynamic bendings, along with torsion, were considered, whereas the lengthwise compressibility was excluded. The system was shown to be fully observable, and due to the nature of the FE method, the positions were estimated from the velocity measurements. The proposed estimation scheme was based on the angular velocity measurements by strap-on MEMS IMU sensors that are suitable to be used in heavy-duty mobile machines. However, the force and moment due to the load are also required as inputs to the observer model, which may prove challenging to achieve for complex dynamic systems. Nonetheless, the FE model can relatively easily be adapted to cover more complex structures, and the handling of the load forces and moments (and flexural DOF) is simple within the model itself.

The Cartesian coordinates along the flexible link were formulated based on rigid body forward kinematics and the estimated deflections. In order to validate the observer's performance, an OptiTrack motion capture system was used as a ground-truth reference to track the respective points along the link in Cartesian space. To validate the torsional angle, the pose of the tip was captured while using an asymmetric tip mass. Actual material parameters were used in the FE equations, which was not achieved in [19]. The initial values of the estimated positions and their respective reference measurements were fully matched for the best comparison of the dynamic behavior.

The experimental results clearly demonstrate that the proposed method can capture the dynamic behavior of the flexural DOF relatively accurately due to model input signals from the IMUs, while the force and moment inputs mostly affect the initial (static) values. Future studies will focus on extending the state estimation for n-DOF flexible-link manipulators and on their environmental contact force control. It may also be interesting to test this method with soft robotics.

ACKNOWLEDGMENT

This work was supported by the Academy of Finland under the project "CPS-based supervision and control of flexible link manipulators," grant no. 294915.

REFERENCES

- [1] G. Zhu, T. Lee, and S. Ge, "Tip tracking control of a single-link flexible robot: A backstepping approach," *Dynamics and Control*, vol. 7, no. 4, pp. 341-360, 1997.
- [2] J.-W. Huang and J.-S. Lin, "Backstepping control design of a single-link flexible robotic manipulator," *IFAC Proceedings Volumes*, vol. 41, no. 2, pp. 11 775-11 780, 2008.

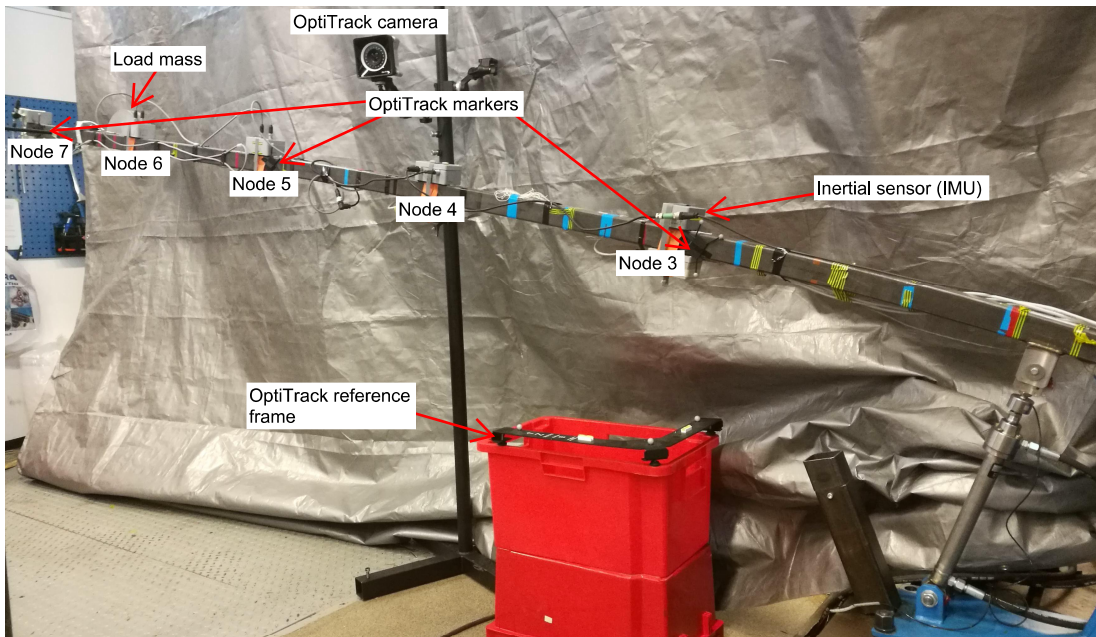


Fig. 2. The experimental 1-DOF (lift actuated) manipulator. The OptiTrack hardware for reference measurements is also shown, albeit not in the actual measurement configuration as the hardware did not fit in the frame. The reference frame was used to set the world frame for the cameras, which then tracked the markers placed along the flexible link with respect to the world frame. Static offsets in the world frame and marker placements were accounted for in OptiTrack Motive optical motion capture software, which was used to read, preprocess, and send data to a dSPACE real-time control PC.

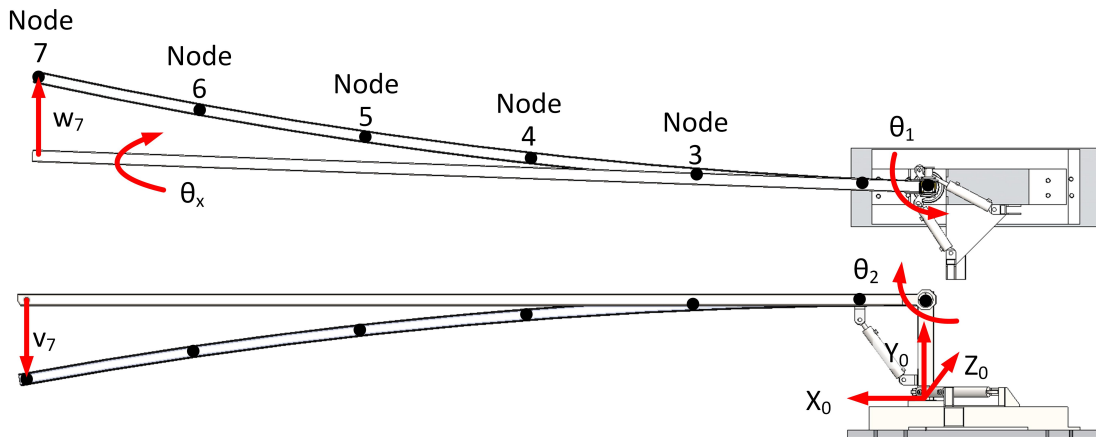


Fig. 3. A schematic of the experimental 2-DOF (lift and turn actuated) manipulator. The upper figure is taken directly from above and illustrates lateral motion. The lower figure is taken directly from the side and illustrates vertical motion. In this work, the flexible link was divided into six finite elements, yielding seven nodes (illustrated by the black dots). Vertical deflection at the tip is denoted by v_7 , lateral deflection at the tip is denoted by w_7 , and the rotational deformation angle due to torsion is denoted by θ_x . The world coordinate system is located at the base of the pillar.

- [3] J. F. Peza-Solis, R. Castro-Linares, and G. Silva-Navarro, "Backstepping-like control using sliding modes for a single flexible-link robot," in *Control and Automation (ICCA), 2011 9th IEEE International Conference on*. IEEE, 2011, pp. 268–273.
- [4] W.-H. Zhu, C. Lange, and M. Callot, "Virtual decomposition control of a planar flexible-link robot," *IFAC Proceedings Volumes*, vol. 41, no. 2, pp. 1697–1702, 2008.
- [5] E. Pereira, S. S. Aphale, V. Feliu, and S. R. Moheimani, "Integral resonant control for vibration damping and precise tip-positioning of a single-link flexible manipulator," *IEEE/ASME Transactions on Mechatronics*, vol. 16, no. 2, pp. 232–240, 2011.
- [6] B. Siciliano and O. Khatib, *Springer Handbook of Robotics - Ch. 11: Robots with Flexible Elements*. Springer, 2016.
- [7] C. T. Kiang, A. Spowage, and C. K. Yoong, "Review of control and sensor system of flexible manipulator," *Journal of Intelligent & Robotic Systems*, vol. 77, no. 1, pp. 187–213, 2015.
- [8] Y. Sakawa and Z. H. Luo, "Modeling and control of coupled bending and torsional vibrations of flexible beams," *IEEE transactions on automatic control*, vol. 34, no. 9, pp. 970–977, 1989.
- [9] Z.-H. Luo, "Direct strain feedback control of flexible robot arms: New theoretical and experimental results," *IEEE Transactions on Automatic Control*, vol. 38, no. 11, pp. 1610–1622, 1993.
- [10] M. T. Hussein and D. Söffker, "State variables estimation of flexible link robot using vision sensor data," *IFAC Proceedings Volumes*, vol. 45, no. 2, pp. 193–198, 2012.
- [11] Y. Xu and E. Ritz, "Vision based flexible beam tip point control," *IEEE Trans. Control Syst. Technol.*, vol. 17, no. 5, pp. 1220–1227, 2009.
- [12] K. Oberfell and W. J. Book, "End-point position measurement of long-

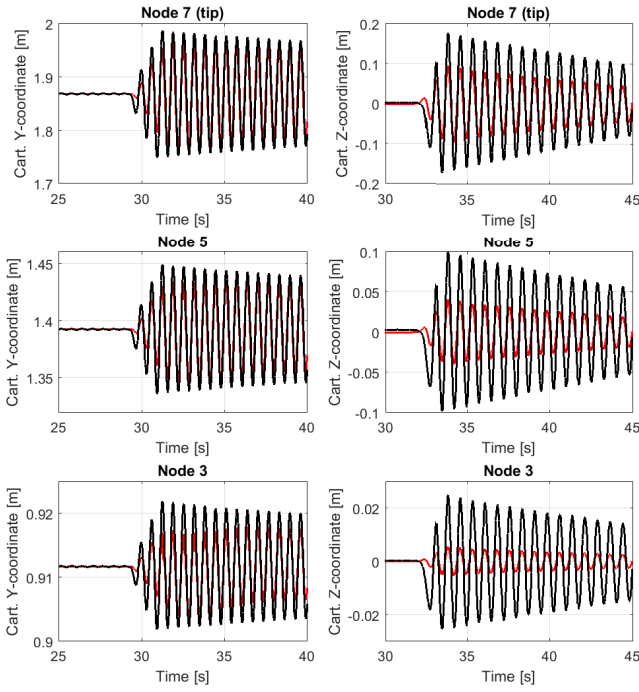


Fig. 4. Free vibration of the flexible link using a 20 kg tip mass. The plots in the left column demonstrate vertical free vibration at three points along the link, whereas the plots in the right column demonstrate lateral free vibration at the three respective points along the link. The measurements are expressed in Cartesian space, and separate measurements were conducted for both bending directions. The black lines represent the OptiTrack reference measurements, and the red lines denote the estimates.

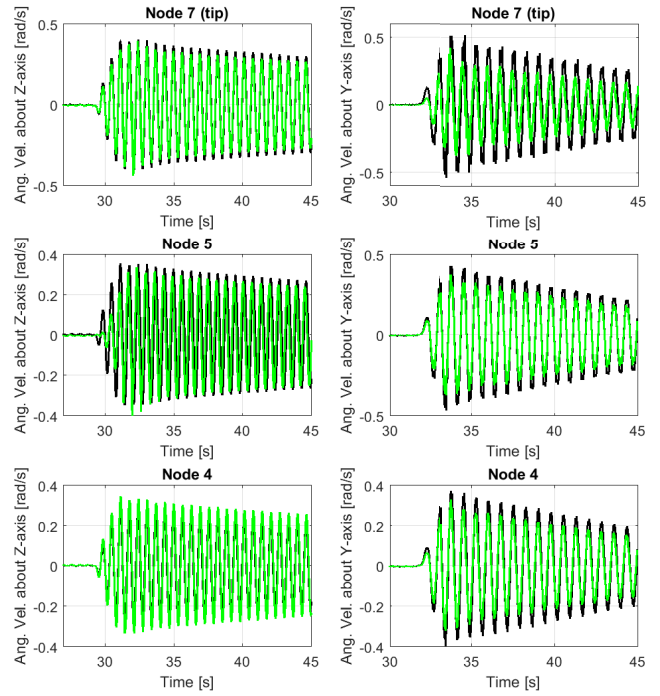


Fig. 5. Free vibration of the flexible link using a 20 kg tip mass. The plots in the left column demonstrate the angular velocities measured from the link's Z-axis (vertical free vibration) at three points along the link, whereas the plots in the right column demonstrate the angular velocities measured from the link's Y-axis (lateral free vibration) at the three respective points along the link. Separate measurements were conducted for both bending directions. The green lines represent the estimated angular velocities, and the black lines denote the IMU measurements.

reach flexible manipulators." Georgia Institute of Technology, 1994.

[13] —, "Vision sensing for control of long-reach flexible manipulators." Georgia Institute of Technology, 1996.

[14] N. Rotella, S. Mason, S. Schaal, and L. Righetti, "Inertial sensor-based humanoid joint state estimation," in *Robotics and Automation (ICRA), 2016 IEEE International Conference on*. IEEE, 2016, pp. 1825–1831.

[15] X. Xinjilefu, S. Feng, and C. G. Atkeson, "A distributed mems gyro network for joint velocity estimation," in *Robotics and Automation (ICRA), 2016 IEEE International Conference on*. IEEE, 2016, pp. 1879–1884.

[16] J. Koivumäki, J. Honkakorpi, J. Vihonen, and J. Mattila, "Hydraulic manipulator virtual decomposition control with performance analysis using low-cost mems sensors," in *Advanced Intelligent Mechatronics (AIM), 2014 IEEE/ASME International Conference on*. IEEE, 2014, pp. 910–917.

[17] J. Vihonen, J. Honkakorpi, J. Tuominen, J. Mattila, and A. Visa, "Linear accelerometers and rate gyros for rotary joint angle estimation of heavy-duty mobile manipulators using forward kinematic modeling," *IEEE/ASME Trans. Mechatronics*, vol. 21, no. 3, pp. 1765–1774, 2016.

[18] J. Vihonen, J. Mattila, and A. Visa, "Joint-space kinematic model for gravity-referenced joint angle estimation of heavy-duty manipulators," *IEEE Transactions on Instrumentation and Measurement*, vol. 66, no. 12, pp. 3280–3288, 2017.

[19] P. Mäkinen and J. Mattila, "Inertial sensor-based state estimation of long-reach flexible-link manipulators," in *Cybernetics and Intelligent Systems (CIS) and IEEE Conference on Robotics, Automation and Mechatronics (RAM), 2017 IEEE 8th International Conference on*. IEEE, 2017.

[20] O. A. Bauchau and J. I. Craig, *Structural analysis: with applications to aerospace structures*. Springer Science & Business Media, 2009, vol. 163.

[21] Y. Kwon and H. Bang, *The Finite Element Method using MATLAB, 2nd ed.* Boca Raton, FL: CRC Press, 2000.

[22] R. L. Williams, D. A. Lawrence *et al.*, *Linear state-space control systems*. John Wiley & Sons, 2007.

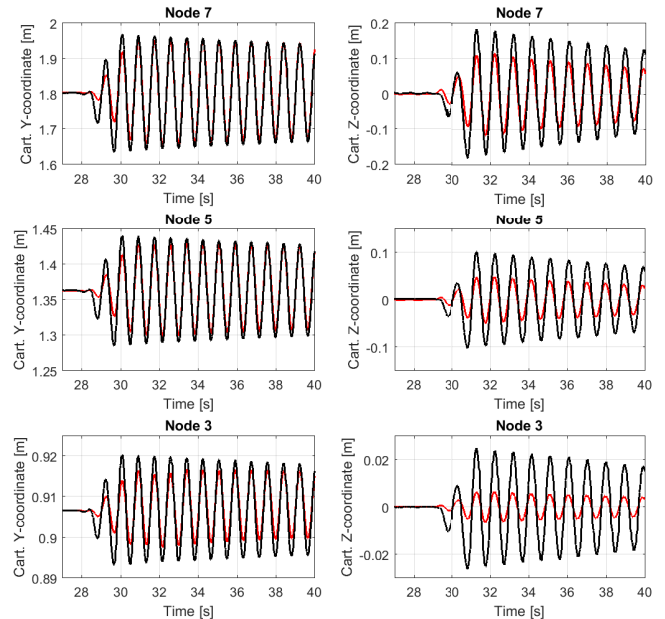


Fig. 6. Free vibration of the flexible link using a 40 kg tip mass. The plots in the left column demonstrate vertical free vibration at three points along the link, whereas the plots in the right column demonstrate lateral free vibration at the three respective points along the link. Separate measurements were conducted for both bending directions. The black lines represent the OptiTrack reference measurements, and the red lines denote the estimates. The measurements are expressed in Cartesian space.

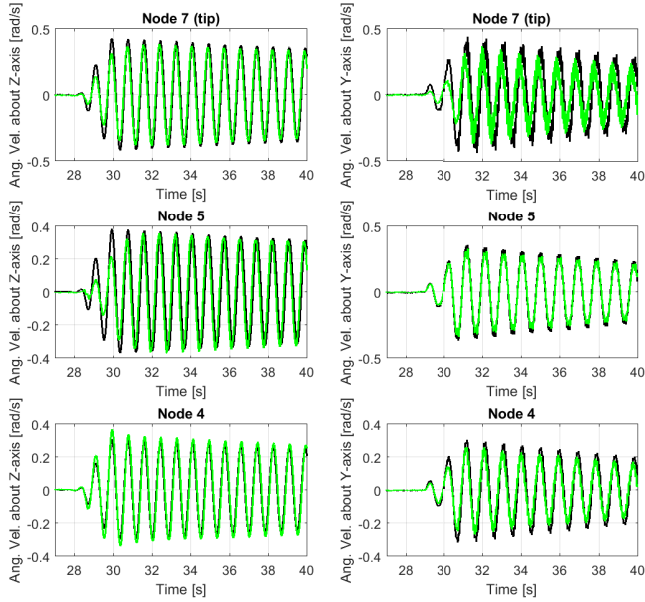


Fig. 7. Free vibration of the flexible link using a 40 kg tip mass. The plots in the left column demonstrate the angular velocities measured from the link's Z-axis (vertical free vibration) at three points along the link, whereas the plots in the right column demonstrate the angular velocities measured from the link's Y-axis (lateral free vibration) at the three respective points along the link. Separate measurements were conducted for both bending directions. The green lines represent the estimated angular velocities, and the black lines denote the IMU measurements.

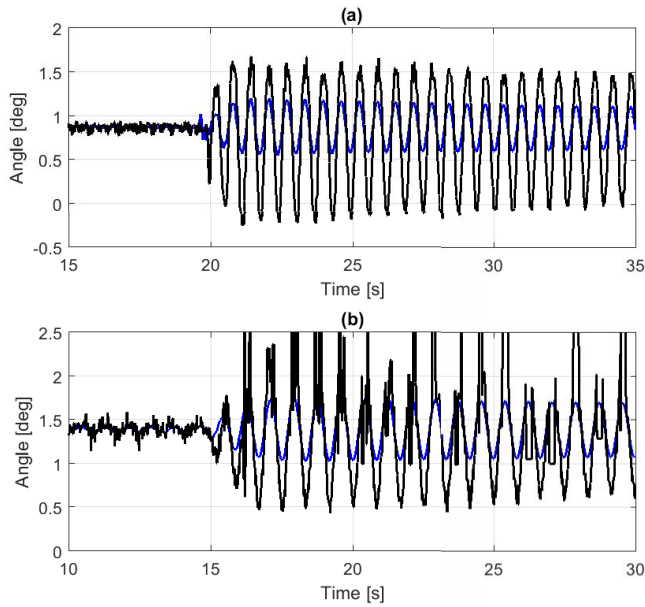


Fig. 8. Rotational angle of the flexible link resulting from torsion. (a) A tip mass of 20 kg was used, and (b) a 40 kg tip mass in the lower. The tip masses were offset by 30 cm with respect to the link's X-axis.

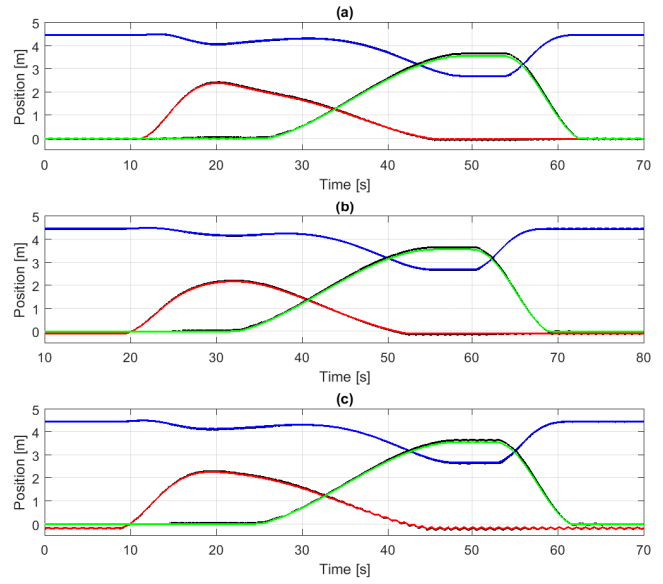


Fig. 9. The end-point coordinates of the 2-DOF manipulator. The blue line denotes the X-coordinate, the red line denotes the Y-coordinate, and the green line denotes the Z-coordinate. Respective OptiTrack reference measurements are all black lines. (a) Tip mass of 20 kg. (b) Tip mass of 40 kg. (c) Tip mass of 60 kg.

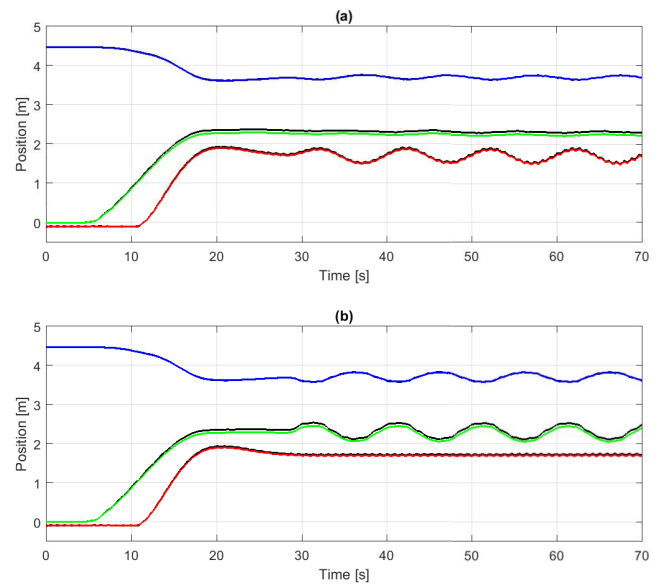


Fig. 10. The end-point coordinates of the 2-DOF manipulator using a 40 kg tip mass. The blue line denotes the X-coordinate, the red line denotes the Y-coordinate, and the green line denotes the Z-coordinate. Respective OptiTrack reference measurements are all black lines. (a) Added a sine wave to the Y-coordinate. (b) Added a sine wave to the Z-coordinate.